Investigation of vapor-deposited amorphous ice and irradiated ice by molecular dynamics simulation

Bertrand Guillot, and Yves Guissani

Citation: The Journal of Chemical Physics **120**, 4366 (2004); doi: 10.1063/1.1644095
View online: https://doi.org/10.1063/1.1644095
View Table of Contents: http://aip.scitation.org/toc/jcp/120/9
Published by the American Institute of Physics

Articles you may be interested in

Control of amorphous solid water morphology using molecular beams. I. Experimental results
The Journal of Chemical Physics **114**, 5284 (2001); 10.1063/1.1350580

Characterization of porosity in vapor-deposited amorphous solid water from methane adsorption
The Journal of Chemical Physics **127**, 204713 (2007); 10.1063/1.2796166

The deposition angle-dependent density of amorphous solid water films
The Journal of Chemical Physics **118**, 364 (2003); 10.1063/1.1525805

Diffraction pattern and structure of amorphous solid water at 10 and 77 °K
The Journal of Chemical Physics **64**, 1106 (1976); 10.1063/1.432298

Molecular dynamics simulation of vapor deposited amorphous ice
The Journal of Chemical Physics **103**, 4678 (1995); 10.1063/1.470655

A general purpose model for the condensed phases of water: TIP4P/2005
The Journal of Chemical Physics **123**, 234505 (2005); 10.1063/1.2121687

PHYSICS TODAY
WHITEPAPERS

ADVANCED LIGHT CURE ADHESIVES

Take a closer look at what these environmentally friendly adhesive systems can do

READ NOW

PRESENTED BY
MASTERBOND
ADHESIVES | SEALANTS | COATINGS

HTML ABSTRACT + LINKS

Investigation of vapor-deposited amorphous ice and irradiated ice by molecular dynamics simulation

Bertrand Guillot[a] and Yves Guissani
Laboratoire de Physique Théorique des Liquides, Université Pierre et Marie Curie, UMR CNRS 7600, Boite courrier 121, 4 Place Jussieu—75252 Paris Cedex 05—France

(Received 7 October 2003; accepted 2 December 2003)

With the purpose of clarifying a number of points raised in the experimental literature, we investigate by molecular dynamics simulation the thermodynamics, the structure and the vibrational properties of vapor-deposited amorphous ice (ASW) as well as the phase transformations experienced by crystalline and vitreous ice under ion bombardment. Concerning ASW, we have shown that by changing the conditions of the deposition process, it is possible to form either a nonmicroporous amorphous deposit whose density ($\sim$1.0 g/cm^3) is essentially invariant with the temperature of deposition, or a microporous sample whose density varies drastically upon temperature annealing. We find that ASW is energetically different from glassy water except at the glass transition temperature and above. Moreover, the molecular dynamics simulation shows no evidence for the formation of a high-density phase when depositing water molecules at very low temperature. In order to model the processing of interstellar ices by cosmic ray protons and heavy ions coming from the magnetospheric radiation environment around the giant planets, we bombarded samples of vitreous ice and cubic ice with 35 eV water molecules. After irradiation the recovered samples were found to be densified, the lower the temperature, the higher the density of the recovered sample. The analysis of the structure and vibrational properties of this new high-density phase of amorphous ice shows a close relationship with those of high-density amorphous ice obtained by pressure-induced amorphization. © *2004 American Institute of Physics.* [DOI: 10.1063/1.1644095]

I. INTRODUCTION

When Burton and Oliver, 70 years ago,[1] showed that the frost resulting from the deposition of water vapor on a cryoplate maintained at liquid nitrogen temperature was amorphous and not crystalline, they could not imagine all the astrophysical implications of this discovery. Nowadays there is every indication that in the outer solar system and in the interstellar medium where the temperature is very low ($T \leqslant 50$ K) the most common form of condensed water is amorphous[2,3] (in the inner solar system condensed water is either liquid, as on earth and likely on Europa, or crystalline). In the last decade a series of rapidly paced discoveries have completely renewed the scenery of the outer solar system.[4] The latter possesses a disklike structure beyond the orbit of Neptune (the Kuiper disk or belt) that contains billions of comets made predominantly of amorphous ice, condensed at temperatures below 50 K, as well as tens of thousands of larger bodies with diameters ranging up to hundreds of kilometres and composed of a rocky core and an icy mantle. Far beyond the Kuiper disk, the Oort cloud extends almost halfway to the nearest star and contains on the order of a billion comets with diameters of a few kilometres or more.[5] It is paradoxical that the periodic entry of some of these objects into the inner solar system is considered nowadays as a serious source of hazard for the life on earth (as a fatal encounter with a kilometer-sized comet), whereas in the early age of the solar system the intense cometary bombardment led to the formation of the oceans and to the spreading of prebiotic organic molecules processed on interstellar grains and at the surface of comets, whose role was likely crucial in the emergence of life.[6] In fact, the building blocks that agglomerate into comets when they are trapped into a protostellar nebula can be observed in dense interstellar clouds.[7] These are dust particles made of silicate grains that are coated with frost composed of water molecules and other volatiles species[8–10] ($CO, CO_2, H_2CO, NH_3, CH_3OH, \ldots$). Depending on their environment (interstellar medium, dense or diffuse clouds, protostellar nebula) the icy grain mantles are energetically and chemically processed by photon irradiation (UV) and charged particle bombardment[11,12] ($p^+, e^-, He^+, \ldots$). The result of this processing is twofold. First, the structure of the ice may be affected (metamorphism, phase transformation) and next, radiation-induced chemical reactions produce radicals and synthesize new molecules.[13,14] For that reason the laboratory study of astrophysical ice analogs is an active field of research[15–21] not only focused on product identification but also to give a comprehensive understanding of ice chemistry in various astrophysical environments. Recently it has been shown[22,23] that the UV photolysis of an amorphous ice deposit composed of H_2O molecules and a percentage of CH_3OH, NH_3, CO, CO_2, and HCN molecules, mimicking the composition of interstellar ice mantles in dense clouds and around protostars, produces spontaneously a number of amino acids.

[a]Electronic mail: guillot@lptl.jussieu.fr

 © 2004 American Institute of Physics

These experiments suggest that prebiotic molecules can be processed in the interstellar medium, and in the absence of liquid water, and could have been delivered to the early earth during the epoch of the intense cometary and meteoritic bombardment.[6] In summary, as long as water ice at astrophysical conditions (very low temperature and pressure) is concerned, it is important to understand in detail the properties of amorphous ice when condensed in the conditions prevailing in the interstellar medium, and especially the role played by the temperature of condensation and the modifications induced upon heating. Furthermore, the elucidation of the effects caused by photon irradiation and ion bombardment on the structure of amorphous ice, effects which are barely known at present, may help to understand the complex chemistry taking place in interstellar ices.

Since Burton and Oliver, many experimental studies have been devoted to the elucidation of the thermodynamic, structural, and dynamical properties of vapor-deposited amorphous ice (in the following we will use the common acronym ASW for amorphous solid water). Thus, it has been reported[24,25] that, on heating, ASW exhibits a glass–liquid transition near 136 K before crystallizing into cubic ice upon further heating to 150 K. The advent of various methods in the 1980s[26] for vitrifying pure liquid water allowed a demonstration of the similarity of behavior between ASW and hyperquenched glassy water (HGW) in the glass–liquid transition region.[27] However, at lower temperatures (typically 10–100 K), a number of studies[28–32] have shown that thermodynamically, structurally, and dynamically, ASW is distinct from glassy water obtained from the liquid phase. In fact, it turns out that the morphology, and hence the properties of a vapor-deposited amorphous film, is strongly dependent on the experimental conditions. Thus, the use of a supersonic flow of water molecules for deposition[33] causes the formation of clusters in the gas phase while condensing on the cryoplate and gives rise to a highly porous material with a large number of pores and voids. On the other hand, the condensation of water monomers from baffled flow will give a nonporous amorphous deposit. In fact, further investigations have shown that vapor pressure, substrate temperature and the nature of the substrate play a role on the structure of ASW. For instance, increasing the vapor pressure, and hence the growth rate, tends to increase the porosity of the ice film. In the same way a higher porosity is favored by a lower temperature of deposition.[34,35] On the other hand, the nature and the morphology of the substrate[36,37] may have an effect on the ice structure (corrugation) and on the onset of the amorphous–crystal transition at temperatures around Tg. Nevertheless, there is a strong dispersion of the results in the literature and only recently has the main source of conflict been identified. Thus, a series of studies[38–40] has shown that the morphology of ASW grown by vapor deposition is found to depend strongly upon the angular distribution of the water molecules impinging the substrate surface. At normal incidence a well-collimated molecular beam produces a dense nonporous solid ($\rho=0.94$ g/cm^3) while at glancing incidence, the deposit is highly porous with an average density that can be as low as 0.16 g/cm^3. These results allow one to understand why the (very common) use of a noncollimated effusive beam with a large angular distribution (called background deposition) leads to ASW samples of various porosity from one author to another. Moreover, the role played by the deposition temperature is found very significant, the lower the temperature, the lower the density of the ice film. By contrast, experiments conducted with collimated beams at normal incidence show no appreciable temperature dependence.[41]

Another source of discrepancy between some data comes from the way the density of the amorphous deposit is measured. Diffraction techniques using x-ray, electron, or neutron sources measure the intrinsic density of the material whereas optical interference techniques lead to the effective or average density including pores and voids, a density value that can be much lower than the former one. Thus, it has been reported in the literature by several independent groups using x-ray and electron diffraction experiments[42–44] that ASW obtained by vapor deposition at very low temperature ($T\leqslant 30$ K) presents a high intrinsic density (≈ 1.1 g/cm^3), a high-density amorphous phase that transforms sluggishly into a low-density phase (≈ 0.94 g/cm^3) upon heating in the temperature range 40–70 K.[44] Moreover, the structure of this high-density amorphous phase is characterized by an interstitial peak around 3.4 A on the oxygen–oxygen pair distribution function. This feature is the signature of a higher coordination number in the first shell of neighbors with respect to crystalline ice (5 instead of 4). However, the formation of a high-density amorphous phase made by vapor deposition is controversial in the literature while that obtained by pressure-induced amorphization of hexagonal or cubic ice, called HDA ice,[45] is well established (for a detailed discussion see our companion paper[46] and references therein). Thus the vibrational spectrum provided by incoherent inelastic neutron scattering[47] (IINS) leaves little doubt about the nonequivalence between high-density amorphous (HDA) ice and ASW deposited at very low temperature. More precisely, the libration band (orientational oscillation) observed in IINS spectra of ASW[31,47] is found to be located between that of HDA ice and that associated with glassy water (HGW). When ASW is annealed around Tg ($\sim$136 K), its libration band becomes identical to that of HGW.[32] Other spectroscopic studies using infrared absorption[48,49] show that ASW deposited at very low temperature is indeed spectrally distinct from annealed ASW. In summary, the vibrational spectroscopies that probe essentially the local environment around each molecule and are less sensitive to the porosity of the material (by contrast with optical interference techniques), indicate that ASW deposited at low temperature is structurally different from HDA ice and converts into HGW after annealing around Tg. On the other hand, keeping in mind the above discussion, it is puzzling that electron diffraction data[44] on ASW deposited below 30 K exhibit diffraction peaks and oxygen–oxygen radial distribution functions very similar to that observed with HDA ice (see Fig. 2 of Ref. 44(b)). The situation becomes even more complicated if one emphasizes that electron microscopy studies[43,50] have shown that when electron irradiation is applied to a sample of ASW deposited at a high enough temperature, it converts into a high-density form provided that the energy dose is

sufficient. In fact, the higher the temperature of irradiation, the higher the electron dose required for the low-density–high density transformation. Consequently, it could be that at very low temperature ($T \sim 10$ K) that the electron dose required to perform an electron diffraction experiment is sufficient to promote the high-density form of ASW.

The effects of irradiation on the structure of water ice have been confirmed, since then by several studies using UV photons,[51] protons,[52] and ions.[53] The structural modifications revealed by electron diffraction scattering[51] and infrared absorption[52,53] show that crystalline ice is amorphized by irradiation whatever the nature of the particles when $T \leqslant 80$ K (above this temperature the crystal is resilient). Furthermore, the resulting amorphous phase seems to be altered by a further irradiation although the alteration cannot be assigned unambiguously to the appearance of a high-density phase. Actually, at the present time, the modifications induced by irradiation on the structure and properties of amorphous ice are still little known and because of their potential astrophysical implications, it deserves to be investigated with more scrutiny. This is one of the objectives of the present study.

The other objective is to investigate the structure, thermodynamic, and vibrational properties of vapor-deposited amorphous ice by molecular dynamics (MD) simulation. One guideline of our study is to simulate as realistically as possible the experimental conditions encountered in the literature and that have a strong influence on the morphology and properties of the amorphous deposit. In particular, special attention will be devoted to the deposition at very low temperature in order to obtain some new clues about the aforementioned controversy concerning the hypothetical relationship between ASW and HDA ice. Few simulation studies on ASW made by vapor deposition have been reported in the literature. The main works are those of Buch *et al.*,[54] who studied by MD calculations the condensation of a few hundreds of water molecules on an initial embryo of cubic ice ($N = 10$ molecules) in order to shed some light on the structure of the resulting condensate. It was found that water molecules can exhibit a coordination number between 2–5, less coordinated molecules being those present at the free surface. A restructuring of the amorphous condensate with increasing temperature was also reported. In another study, Essmann and Geiger[55] simulated the slow deposition of water molecules on a substrate made of Lennard-Jones particles. Although the simulation was aimed to obtain a dense and homogeneous deposit, it was found to be deeply fissured, the denser part being that in contact with the substrate. Hence, it is difficult to draw an unambiguous conclusion concerning the existence of a high-density form for ASW deposited at low temperature. In a related work Wilson *et al.*[56] in depositing water molecules on a lamella of bulk amorphous ice (prepared from a quenched configuration of the liquid) obtained a microporous amorphous film whose the density profile varied strongly with the distance to the substrate. It was also found that the microporosity decreases when the water molecules impinge on the surface with a higher thermal velocity, and that the deposit becomes denser upon heating. Moreover, the search for a high-density phase was still unsuccessful.

Whatever the case, the above simulation studies had a limited scope and did not pretend to be exhaustive and fully realistic with respect to experimental conditions. By contrast, the purpose of the present study is to evaluate the various properties of simulated ASW in such a way as to be able to compare them quantitatively with available experimental data and notably with other forms of amorphous ice. Thus, the parameters used in our simulations (force field, number of water molecules, long range corrections, geometry of the simulation cell) are the same as those used in a previous study (see the companion paper[46]) dealing with pressure-induced amorphous ice and hyperquenched glassy water. So we will be in a position to compare the properties of all these amorphous ices on the same footing. In Sec. II the simulation method employed to obtain amorphous ice by vapor deposition is presented and the results discussed. Section III is devoted to irradiation effects on amorphous and crystalline ice by ion bombardment. The main results of this study are summarized in Sec. IV and put in perspective with the present state of the field.

II. VAPOR-DEPOSITED AMORPHOUS ICE

A. Computational details

An important step of a MD calculation is the determination of the force field describing the molecular interactions. It exists in the literature a vast choice of model potentials for water (for a review see Ref. 57), which are, in general, adjusted to reproduce the properties of liquid water near ambient conditions. Among these models, the three-site models are the most commonly used in simulation works because of their good accuracy to computer cost ratio. All the calculations presented here are based upon an empirical pair potential recently introduced by us.[58] The novelty of this three-site model is to use diffuse charges in addition to point charges on oxygen and hydrogen atoms in order to account for electronic penetration effects. Unlike most of the existing nonpolarizable models it does not require an enhanced dipole moment to reproduce accurately liquid state properties. In a previous study[46] we have used this model to simulate by MD the other forms of amorphous ice namely, HDA ice obtained by pressure-induced amorphization of cubic ice at low temperature, LDA ice resulting from the transformation of HDA ice upon heating, and glassy water (HGW) issued from a rapid cooling of the liquid. The overall agreement between the simulation results and a number of experimental properties of these amorphous ices is quite good, which indicates that the selected interaction potential is sufficiently realistic to describe low-temperature water in detail.

As far as vapor deposition is concerned, another important parameter of the simulation is the nature of the substrate on which the water molecules are condensed. Experimentally, different substrates are used in the literature to grow an amorphous ice film from the vapor (e.g., Au, Si, Ru, SiO_2, Al_2O_3,…). Several studies[36,37,48] have shown that the roughness of the substrate surface, its chemical composition, its hydrophilicity (or hydrophobicity) can play a role in the mor-

phology and microporosity of the amorphous deposit. In particular, the effect induced by the substrate on the deposit affects the first few ice monolayers (ML) with weakly perturbing substrate (hydrophilic) and may extend up to 50 MLs with a highly hydrophobic surface.[36] Since our computer resources only allow one to simulate very thin amorphous ice films (~10 MLs), it is important to choose the less perturbing substrate in this context. So discarding substrates modeled by hard spheres, Lennard-Jones particles, or a structureless surface (wall) whose corrugation effect is not easy to estimate, we have preferred to use as substrates a lamella of glassy water (HGW) and a lamella of cubic ice, respectively. As a matter of fact, because of the presence of dangling OH bonds and oxygen atoms protruding from the free surfaces of these lamella, it is expected that the impinging water molecules can adsorb easily on these very hydrophilic surfaces. Moreover, it is important to check if the substitution of a crystalline surface of cubic ice (001) to that of glassy water has an effect on the morphology of the deposit, especially in varying the temperature of deposition, if one remembers that every amorphous ice, whatever its type, transforms into cubic ice beyond the glass transition temperature. Last but not least, the lamella of glassy water and that of cubic ice will play the role of benchmarks when it will be the question to describe the properties of vapor-deposited amorphous ice.

In practice, the MD calculations were performed in the microcanonical ensemble (NVE) with periodic boundary conditions in all three dimensions. The long range interactions were handled by an Ewald sum adapted to the lamellar geometry investigated here (see below and Ref. 59). The equations of motion were solved with the Verlet algorithm in using a small time step (0.5 fs) to ensure an optimal conservation of energy. We have first prepared the two lamella acting as a substrate. Since the procedure is essentially the same as that described in the previous study,[46] we only summarize it briefly. A sample of liquid water composed of 512 molecules contained in a parallelepipedic box ($l_Z = 2l_X = 2l_Y \sim 40$ A) is simulated at ambient conditions (0.997 g/cm^3 and 298 K). The simulation box is next extended along the Z direction ($l_Z = 8l_X = 8l_Y \sim 160$ A) in order to provide two empty spaces, one on each Z side of the liquid slab. After equilibration, this geometry allows one to simulate the coexistence between a liquid slab at the center of the box and the vapor emanating from it. Hence, a change of temperature is sufficient to follow the saturation line (notice that $N = 512$ molecules is large enough to avoid any significant size dependence in the results[59]). In the present case, starting from an equilibrated sample at room temperature (at this temperature there is virtually no molecules in the gas phase due to the very low pressure at saturation) and in applying a sufficiently rapid cooling rate, one can go through the supercooled states to reach the glassy state before crystallization takes place. However, in a MD simulation the cooling rate accessible with the computer resources is so large that crystallization is generally avoided (for a detailed discussion see Ref. 46). In applying a cooling rate of 10^{10} K/s (this is done by rescaling periodically the velocities of the molecules by a very small factor to ensure thermal equilibrium during the cooling), the liquid slab undergoes a glass transition around 172 K (see also Ref. 46). Although this latter value is significantly higher that the value assigned to the glass transition temperature in water (~136 K; see Ref. 27), the thermodynamic properties, the structure, and the vibrational density of states of our simulated glassy water are in quite good agreement with the experimental data for hyperquenched glassy water.[46] In the following we will use the two opposite Z faces of the glassy lamella as cold surfaces for deposition.

For the crystalline lamella, we have prepared a parallelepipedic sample of cubic ice (diamond-type lattice) composed of $N = 432$ molecules ($l_Z = 2l_X = 2l_Y \sim 38$ A), that is 24 crystalline planes perpendicular to the Z direction, and in leaving an empty space on each side of the crystal ($l_Z = 8l_X = 8l_Y \sim 152$ A). The density of the crystal at zero pressure varies between 0.98 g/cm^3 near 0 K and 0.945 g/cm^3 at 200 K, as compared with around 0.93 g/cm^3 for real cubic ice at 150 K. Its lattice energy at 0 K is -55.9 kJ/mol, which compares well with an experimental evaluation around -57.3 kJ/mol (see Ref. 46 for a discussion). Furthermore, as our cubic ice lamella melts above 215 K, it is well suitable for deposition over a rather large temperature range (0–200 K).

In the Introduction we emphasized that experimental studies on vapor-deposited amorphous ice[34–41] stressed the influence of the experimental conditions (temperature of deposition, intensity of the vapor flux, angular distribution of the incident molecular beam flux) on the ASW film morphology (porosity). Consequently, we have varied our simulation conditions for vapor deposition to estimate their influence on the deposit. Nevertheless, one has to be aware of the very high rate of deposition imposed by our limited computer resources. Thus the condensation of a few hundreds of molecules on an area of 400 A^2 requires a rate of deposition of the order of a few m/s to be tractable, as compared with experimental deposition rates about 10^{-2}–10^2 A/s. So in a real experiment the time between two successive events (a molecule landing on the surface) at the same location is very long at the molecular time scale while it can be very short in the simulation, which could bias the results. In searching to minimize this problem we have, in a first attempt, inserted two water molecules into the simulation box: one in each free volume situated on both sides of the lamella. The position of molecule 1 was chosen randomly (as well as its orientation) and the position of molecule 2 deduced by symmetry ($x_2 = -x_1$, $y_2 = -y_1$, $z_2 = -z_1$). The kinetic energy of the incident molecules was set equal to 300 K with an impulsion pointing perpendicularly to the facing cold surface or distributed in a cone of 60°. During the simulation run the equations of motion of the incident molecules and those of the molecules composing the lamella are solved. After a quasifree flight, the incident molecules hit the surface of the lamella and the velocities of the substrate molecules are rescaled to maintain a constant temperature of the lamella. After about 1000 MD steps, the impacting molecules are thermalized by collisional de-excitation and become adsorbed on the surface (notice that we have never observed a rebounding of a molecule impinging on the surface). The procedure is started all over again at regular intervals in introducing two

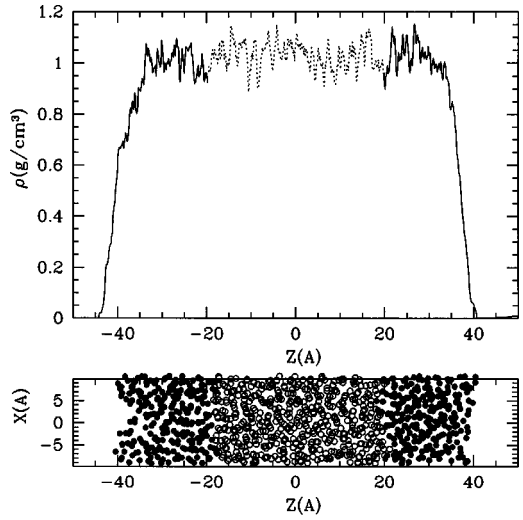

FIG. 1. Density profile (top panel) and snapshot (bottom panel) of the amorphous film deposited on the glassy lamella at 100 K. In the upper panel, the dotted line corresponds to the average density of the substrate and the full line to that of the deposited film as a function of the Z coordinate. In the lower panel the empty circles represent the positions of the centers of mass of the water molecules of the substrate and the full circles are those of the deposit.

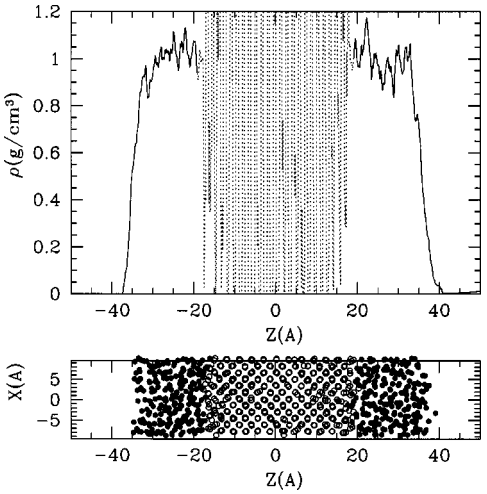

FIG. 2. As in Fig. 1 but for the deposition on cubic ice at 100 K.

new molecules in the empty spaces of the simulation box. However, to speed up the rate of deposition, the periodicity chosen for introducing new incident molecules is such that several molecules are traveling at the same time in each free volume of the simulation box. The procedure is ended when 512 water molecules were deposited on the glassy lamella (256 molecules on each side) and 432 water molecules on the crystalline lamella, respectively. But with this method it became rapidly obvious that the rate of deposition is too high and produces a very porous film whatever the angular distribution of the incident molecules. In fact, it happens frequently that several molecules strike the same area of the surface almost simultaneously. Indeed, during their free flight, the incident molecules are, on average, separated by 10 A (or less), and consequently they interact and tend to form clusters in the gas phase before landing on the interface. The net result is the formation of a highly porous film. Obviously, at the scale of our simulation box this microporosity only extends over a few molecular diameters and has nothing to do with macroporosity that is sometimes observed experimentally with fluffy or needlelike morphology for the deposit. So in order to produce a nonporous deposit each new incoming molecule is dropped with an initial velocity equivalent to 300 K at a random location in the (x,y) plane but at a z position above the surface which does not exceed one molecular diameter from the nearest molecule of the substrate. Moreover, all insertions of a new molecule in the immediate vicinity of a previous deposition event are rejected if the thermalization process of the latter one is not completed (this lasts about 1000 MD steps). This procedure guarantees that each molecule adsorbs on the surface independently from each other and that the time available for thermalization is sufficient before the molecule is buried by other incident molecules. For illustration, we present in Figs. 1 and 2, the density profile and a snapshot of the simulation cell at the end of a deposition process performed at 100 K on a glassy lamella (Fig. 1) and on a lamella of cubic ice (Fig. 2), respectively. One can see on the two figures that the deposit (one on each side of the corresponding lamella) is dense whatever the substrate ($\sim$1.0 g/cm^3 on average) and nonporous with a clear free interface. Besides, in Fig. 1, it is virtually impossible to distinguish on the density profile, the glassy lamella (issued from the liquid) from the amorphous deposit. The wiggling aspect of the density profile is due essentially to the small number of molecules composing each z slice ($\sim$40 molecules per 3 A slice) and to the absence of diffusive motions on the time scale of the simulation. Nevertheless the average density evaluated on the total thickness is well defined and accurate (see below).

B. Results

The procedure of deposition was repeated at different temperatures, namely 10, 50, 100, and 150 K on the glassy lamella and 10, 50, 100, 150, and 200 K on the crystalline lamella. It took about 300 ps to deposit 512 molecules and a further equilibration run of 100 ps or more was necessary for energy relaxation. The time evolution of several indicators (density, potential energy, pair distribution functions) showed that no significant evolution of the morphology and properties of the amorphous deposits could be expected by continuing the simulation run (however, it is likely that a much larger system would exhibit a much longer relaxation time). The density of each amorphous film was evaluated by averaging over the thickness of the deposit and in excluding from the counting the first monolayers acting as an interface (vacuum–deposit, and deposit–substrate). The density values as a function of the temperature of deposition are reported in Fig. 3 for the two lamella. The density of the latter ones is also given for comparison. The density of our vapor-deposited amorphous ice is in the range 0.985–1.035 g/cm^3 and is essentially independent of the temperature. Furthermore, the density of ASW matches that of glassy water (see Fig. 3) and is independent of the nature (amorphous or crystalline) of the substrate. Another important result is that there is no evidence for a high-density amorphous phase when

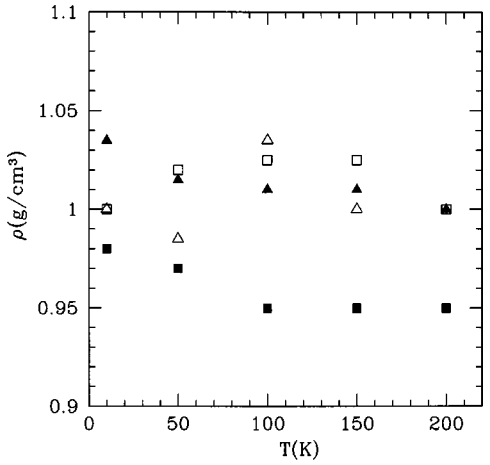

FIG. 3. The evolution of the density of the deposit with the temperature of deposition. The empty triangles are for the deposition on the glassy lamella and the empty squares are for the deposition on cubic ice, while the full triangles and full squares correspond to the density of the glassy and crystalline substrate, respectively.

water molecules are deposited at very low temperature (e.g., 10 K). On the other hand, our simulation results are in agreement with experimental data[38–40] using deposition conditions that promote the formation of nonporous ice films (normal incidence of the incident flux, effusive beam, very low operating pressure).

As reviewed previously, the use of background deposition (or omnidirectional deposition) at very low temperature or the recourse to supersonic flow conditions for the molecular beam generally produces a highly porous amorphous deposit characterized by a density much lower than 1.0 g/cm^3. In the case of a supersonic beam, water clusters already form in the gas phase, because of the cooling generated by the supersonic expansion, before condensing on the cryoplate. In order to reproduce this cluster formation by MD simulation, we have proceeded in the following way. In an empty simulation cell (where $l_Z = 8l_X = 8l_Y \sim 160$ A), we introduce at each Z end of the box a water molecule at a random location in the (x,y) plane. At these molecules are assigned an initial velocity corresponding to a temperature of 30 K, with a direction parallel to the Z axis and pointing toward the middle of the cell. This procedure is repeated every 2500 MD steps until a total number of 512 molecules is inserted (256 on each side of the box). During the insertion process, the velocities of the molecules are periodically rescaled to maintain a constant temperature of the system (30 K). This method allows one to grow two independent water clusters made of 256 molecules, whose shape is roughly cubic (the use of periodic boundary conditions transforms this cube into a slab perpendicular to the Z axis). Actually, during the insertion process, the molecules are quite close to each other (a few molecular diameters) and strongly interact. In maintaining the temperature of the system as low as 30 K (a temperature typical of supersonic flows and encountered in the interstellar medium), the water molecules rapidly form stable clusters, which, by aggregation, build up a large cluster (due to the initial conditions, each cluster is dragged at a very low speed toward the center of the box). The latter is highly

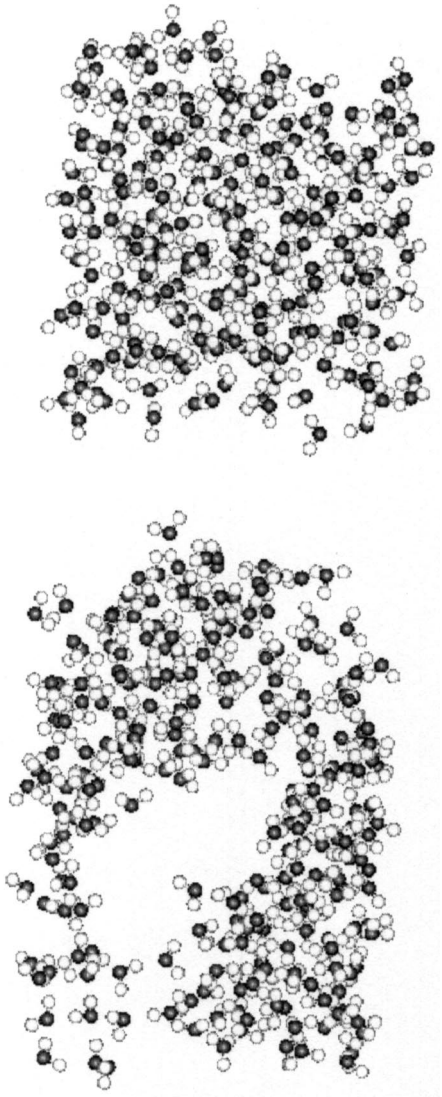

FIG. 4. The snapshot of a nonporous deposit at 10 K (upper picture) and of a porous cluster at 30 K (lower picture). Note that both amorphous systems are composed of the same number of molecules ($N = 256$).

porous with a rough surface and exhibits an average density around 0.62 ± 0.06 g/cm^3 (evaluated from four independent clusters), a value in excellent agreement with experimental data obtained with omnidirectional deposition at low temperature.[34,35,40] A snapshot of one of these clusters is shown in Fig. 4 and is compared with a dense nonporous amorphous deposit. Upon heating the amorphous cluster densifies by local restructuring of the hydrogen bond network that eliminates step by step a number of cavities and voids. The evolution of the density with the temperature is shown in Fig. 5 for a heating rate of 0.1 K/ps (or 10^{11} K/s). One sees that the density increases gradually from 0.62 g/cm^3 to reach the value characterizing nonporous amorphous ice ($\sim$1.0 g/cm^3) only at a temperature well above Tg ($\sim$172 K for our model). In fact, with the heating rate employed, the amorphous ice is not fully relaxed and it is necessary to anneal it isothermally at given temperatures along the heating pathway to evaluate the correct density evolution. The time relaxation of the potential energy and of the density of amorphous ice is presented in Fig. 6 at four different

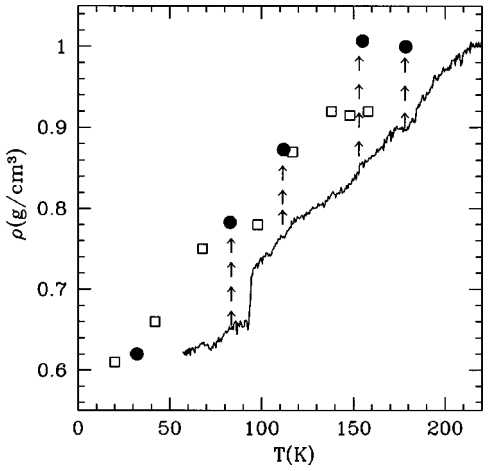

FIG. 5. Evolution of the density of the cluster with the temperature. The full curve corresponds to a heating rate of 0.1 K/ps (see the text) from 55 to 220 K and the full dots after an isothermal annealing at given temperatures (indicated by vertical arrows). Notice that the temperature of formation of the amorphous cluster is 30 K and the corresponding full dot in the figure is for the equilibrated cluster at this temperature. For comparison, the experimental values obtained by Dohnalek *et al.* (Ref. 40) with omnidirectional deposition are also given (empty squares).

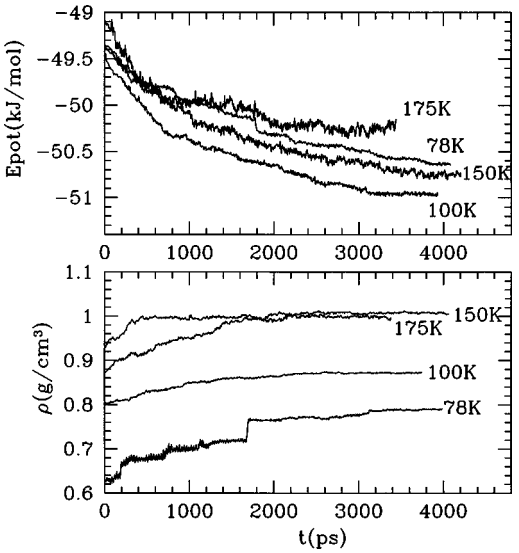

FIG. 6. Time relaxation of the potential energy and density of the amorphous cluster upon isothermal annealing.

temperatures (78, 100, 150, and 175 K). It is noteworthy that several nanoseconds are necessary to relax the structure (the lower the temperature, the longer the time relaxation) and that the ice reconstruction sometimes proceeds by sudden changes (especially visible on the density curve at 78 K) corresponding to the collapse of cavities. This gradual process induced by annealing is well documented in spectroscopic studies.[48,49] The final values of the density for apparently relaxed amorphous clusters are reported in Fig. 5 as a function of temperature (the vertical arrows show the density evolution during an isothermal annealing). The agreement with recent experimental data[40] obtained by omnidirectional deposition is remarkable (see Fig. 5). In particular, the fact that porous amorphous ice becomes fully dense only in approaching Tg is well reproduced by the simulation (as emphasized earlier, Tg$\sim$136 K for real ASW while it is $\sim$172 K in the simulation). On the other hand, the present quantitative agreement suggests that the porosity responsible for the density evolution with temperature in the deposition experiments reported in Fig. 5 is essentially at the scale of a nanometer, as seen in Fig. 4. By contrast, a density much smaller than 0.6 g/cm^3 ($\sim$0.2 g/cm^3 in Ref. 40), as observed in some deposition experiments, is likely the signature of a microporosity whose scale is far beyond that probed by the present simulation (e.g., in Ref. 60).

From a more general point of view, when considering the description of the various forms of amorphous ice, their thermal properties play a central role.[61] The enthalpy associated with ASW obtained by vapor deposition is governed essentially by the potential energy since the PV contribution is negligible. The evaluation of the potential energy by MD is straightforward for the amorphous clusters but merits some comments in the case of the deposits. For the sake of argument, let us consider a model substrate (for instance a wall with a surface potential) on which the molecules are condensing. The potential energy, E, of the deposited film is the sum of two terms, $E_{WW}+E_{WS}$, where E_{WW} is the interaction energy between the N water molecules of the deposit and E_{WS} is the interaction energy between the molecules of the deposit and the substrate. At the thermodynamic limit, E becomes identical to E_{WW} because the ratio E_{WS}/E_{WW} vanishes as $1/N$. But when the thickness of the deposit is of the order of a few tens of monolayers, and if the substrate–water energy per particle (E_{WS}/N) is no longer negligible with respect to the water–water interaction energy (E_{WW}/N), the substrate may have a significant effect on the configuration of water molecules within the deposit. This simple remark explains why experimentally the morphology of amorphous films are occasionally affected by the nature of the substrate,[36,37] a perturbation that may propagate through several tens of monolayers. In the present case, the substrate is a lamella of water ice (glassy or crystalline) of finite thickness ($\sim$24 MLs for cubic ice). The situation is then more intricate since the water molecules forming the deposit modify the configuration of the molecules belonging to the substrate. Hence, the potential energy of the deposit becomes $E=E_{WW}+E_{WS}/2$, the factor 1/2 indicating that the substrate–deposit energy is shared equally between the molecules of the deposit and that of the substrate (correspondingly the interaction energy between the substrate molecules is equal to $E_{SS}+E_{WS}/2$). At the thermodynamic limit (the thickness of the deposit $L\rightarrow\infty$) one recovers the expected result $E=E_{WW}$. In our simulation the thickness of the deposit in the Z direction is proportional to the number N of deposited molecules. In Fig. 7 is shown for illustration, the evolution of the potential energy E (per mole of deposited molecules) of the amorphous film with the number of deposited molecules at 50 K and its decomposition into E_{WW} and E_{WS}, respectively. The key point is that the thermodynamic limit is virtually reached after the deposition of about 60 molecules ($\sim$3 MLs) and that this result is independent of the temperature of deposition (not shown) and of the glassy or crystalline nature of the substrate investigated here. (The very small residual drift exhibited by E in Fig. 7 when N is greater than

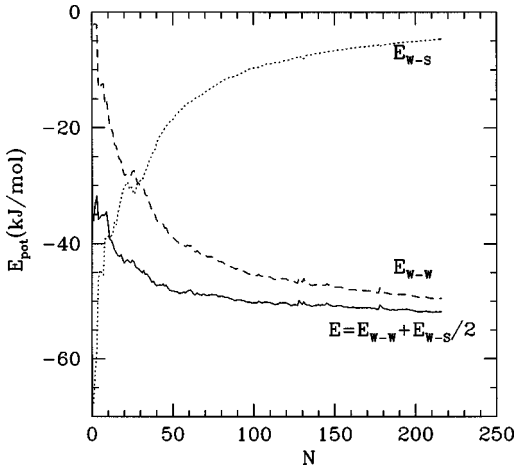

FIG. 7. Evolution of the potential energy (E) of the amorphous film with the number of deposited molecules at 50 K (see the text). The interaction energy between the molecules of the deposit (E_{W-W}) and that between the deposit and the substrate (E_{W-S}) are also shown.

~60 is simply due to the structural relaxation between each deposition event). Actually this result is not unexpected if one notes that a substrate made of water molecules is certainly the least perturbing surface for depositing water molecules. In conclusion, the rapid convergence exhibited by the energy of the deposition justifies *a posteriori* our choice of a lamella of water ice as a substrate.

The evolution with temperature of the potential energy of our simulated samples of amorphous ice, deposit and cluster, are presented in Fig. 8 (notice that, for convenience, a factor equal to 3 RT was subtracted from the potential energy to account for harmonic motions in the amorphous state). For comparison, the potential energy of a lamella of cubic ice is shown as well as the evolution upon rapid cooling (10^{-2} K/ps) of a lamella of water from the liquid phase to the glassy state (see Ref. 46). Since the MD calculations were performed in similar conditions for all these systems, their respective energy can be compared directly with each other. In the case of the amorphous cluster it is obvious in Fig. 8 (see full circles) that its potential energy is much higher than that of glassy water; the lower the temperature, the larger the deviation, and by contrast with the behavior of HGW its energy decreases when the temperature increases, except in approaching Tg, where the slope changes sign. Besides, at the glass transition temperature, the energy of the annealed amorphous cluster and that of HGW become identical to each other, as expected. A similar behavior is observed with vapor-deposited amorphous samples, but their energy values (see full triangles and squares in Fig. 8) are intermediate to that of porous ASW (cluster) and HGW. In this context it must be pointed out that experimentally it is known that vapor deposition produces larger configurational enthalpy than does liquid quenching.[62] Moreover, considering the statistical uncertainties of the calculations, the energy of the amorphous deposits is found to be essentially independent of the morphology (crystalline or glassy) of the substrate. The net conclusion is that our simulated ASW, whether it is porous or nonporous, is energetically different from glassy water except at Tg and beyond, where they match. We will see in the following that the investigation of structural and dynamical properties confirm this finding.

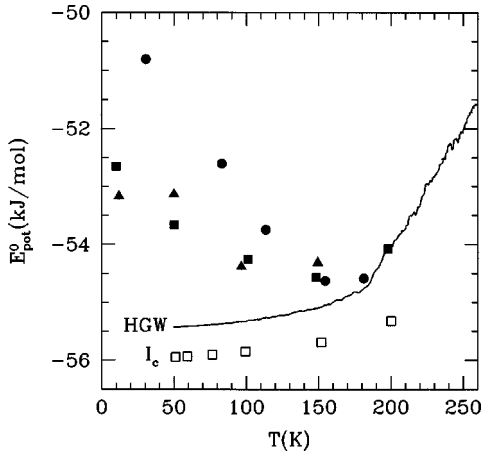

FIG. 8. Evolution of the potential energy with temperature for a variety of amorphous ices. The full triangles correspond to ASW deposited on glassy water (HGW), the full squares correspond to ASW deposited on cubic ice, and the full circles are for the porous cluster annealed at different temperatures. The curve (HGW) represents the evolution of the potential energy when cooling a liquid slab with a cooling rate of 0.01 K/ps. From this energy curve a glass transition temperature around 172 K can be deduced (see Ref. 46). The empty squares represent the energy of cubic ice in the slab geometry investigated here (see the text). Notice that a contribution of 3RT was subtracted from the potential energy to account for harmonic motions in the solid state.

From the experimental point of view, only the heat of crystallization into cubic ice of annealed ASW above Tg is known, which is evaluated[27] around −1.29 kJ/mol at 150 K. The heat of crystallization of our simulated ASW amounts to −0.7 kJ/mol at Tg and −1.3 kJ/mol at 200 K in the supercooled liquid, respectively, in rather good agreement with the aforementioned experimental value. The entropy of our vapor-deposited amorphous ice was evaluated by using the quasiharmonic approximation that relates the entropy to the vibrational density of states (see the footnote[90] in Ref. 46). At 100 K we obtain 3.4 $J\,mol^{-1}\,K^{-1}$ for the excess entropy of dense amorphous ice with respect to cubic ice, as compared with an experimental evaluation[63] amounting to 1.7 ± 1.7 $J\,mol^{-1}\,K^{-1}$ at 150 K. However, it is the Gibbs free energy difference between ASW and cubic ice that was measured from the rate of evaporation of the two condensed phases, $\Delta G = 1.1 \pm 0.1$ kJ/mol. For the same quantity, but at 100 K, we obtain 1.2 kJ/mol in summing up the excess entropic and enthalpic contributions. This is an excellent agreement if one considers that ΔG is weakly temperature dependent between 100 and 150 K, as suggested by the simulation results (not shown). On the other hand, the measurement of the rate of evaporation of amorphous ice has important implications for interstellar ices,[64] and its evolution with temperature is an indication of the ice structure (porosity). Thus, a strong variation of the evaporation rate with temperature and with the conditions of deposition was reported.[65,66] The lower the temperature, the higher the evaporation rate (and ΔG) of ASW with respect to crystalline ice. These observations support the energy–temperature diagram presented in Fig. 8, namely, an important increase of the excess energy of

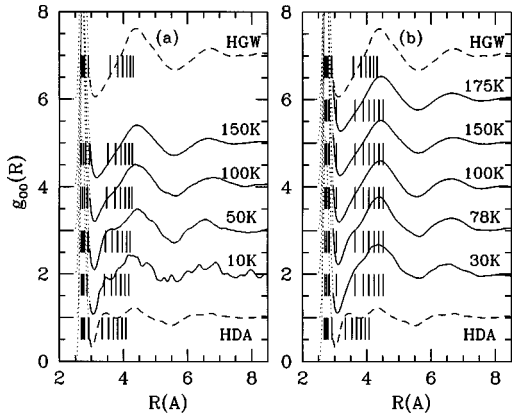

FIG. 9. The oxygen–oxygen pair distribution function for (a) ASW deposited on glassy water at various temperatures and (b) for the amorphous cluster annealed at different temperatures (see the text). The bars indicate the average distance between a central molecule and its ten nearest neighbors in the corresponding amorphous ice. The first peak of $g_{OO}(R)$ is displayed as a dotted line for convenience. The pair distribution functions associated with HDA ice at 50 K and with HGW at 78 K are also shown for comparison (see the text).

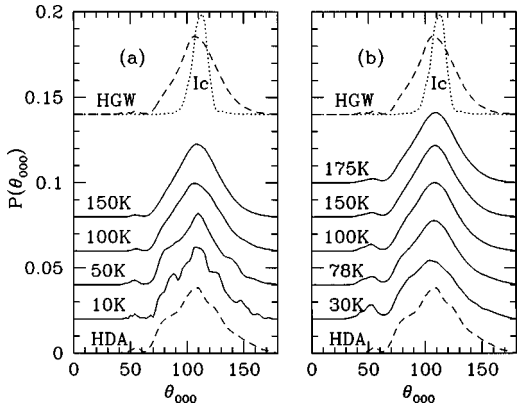

FIG. 10. The angular distribution function for oxygen atoms in (a) ASW deposited on glassy water at different temperatures and (b) in the amorphous cluster annealed at different temperatures (see the text). The angular distribution functions in HDA ice and in cubic ice at 50 K, and in HGW at 78 K are also given for comparison.

amorphous ice at low temperature. In the case of porous ASW like our amorphous clusters, the calculated excess Gibbs energy amounts to 5.0 kJ/mol at 30 K (decomposed into $\Delta H = 5.2$ kJ/mol and $\Delta S = 5.8\ \mathrm{J\,mol^{-1}\,K^{-1}}$) and leads to an evaporation rate eight orders of magnitude larger for the amorph than for the crystal.

One advantage of computer simulations is to make the connection between the thermodynamic properties discussed above and the underlying microscopic structure. Thus we have evaluated the oxygen–oxygen, oxygen–hydrogen, and hydrogen–hydrogen pair distribution functions (pdf) that are the basic functions to interpret the structure data given by x-ray and neutron scattering experiments. In order to minimize the surface effects in vapor-deposited amorphous ice coming from the water molecules located at the interfaces (free or in contact with the substrate) of our samples, we have excluded from the counting those molecules. In Fig. 9(a) is presented the evolution of the oxygen–oxygen pdf with the temperature of deposition. Only the pdf of ASW deposited on the glassy lamella is shown because the corresponding function for the deposit on cubic ice is virtually indistinguishable. Whatever the temperature, the oxygen–oxygen pdf presents a second peak around 4.5 A, which is the well-known signature of the three-dimensional (3-D) hydrogen bond network of water. Besides, the resemblance with the pdf for glassy water (HGW), also presented in Fig. 9(a) for comparison, is striking. However, it is also clear that when the temperature of deposition decreases, a shoulder appears around 3.4 A, a value situated between the two first shell of neighbors. This feature is reminiscent of the interstitial peak characterizing HDA ice obtained by amorphization under pressure of hexagonal or cubic ice (see Sec. IV in Ref. 46 for a detailed discussion). Moreover, it has been shown that the interstitial peak in HDA ice originates from the occurrence of a fifth molecule (nonhydrogen bonded) in the first shell of neighbors surrounding a central molecule. The important point being that the enhancement of the molecular packing (and density) induced by the amorphization process originates from a distortion of the hydrogen bond network without a significant loss of hydrogen bonds. Nevertheless, in the present case, the density of nonporous ASW does not exceed ~ 1.0 g/cm^3 instead of ~ 1.16 g/cm^3 for HDA ice. So, to analyze what is happening in the amorphous deposit, the average position of the ten nearest neighbors around a central molecule is reported in Fig. 9(a) [see the bars superimposed to $g_{OO}(r)$]. The first peak of $g_{OO}(r)$ is composed of the four first neighbors that are well separated from the other ones, indicating that the first shell is essentially occupied by four water molecules all hydrogen bonded to a central one. By contrast, the molecules belonging to the second shell tend to penetrate into the separation with the first shell, the lower the temperature of deposition, the deeper the penetration. Thus the fifth molecule is found responsible for a shoulder around 3.4 A. Complementary information is given by the analysis of the average pair energy between a central molecule and its neighbors, where it is clear (not shown) that the first four neighbors are hydrogen bonded to a central one, the fourth being a little bit less tightly bound, while the fifth molecule and the other ones are nonbonded. In fact, as in the case of HDA ice, the penetration of the fifth molecule in the region separating the two first shells leads to a distortion of the tetrahedral configuration characterizing the first shell. This is illustrated in Fig. 10(a), where the O–O–O angular distribution between the oxygen atom of a central molecule and the oxygen atoms of its four nearest neighbors is shown. The appearing of nontetrahedral configurations around 80° and above 120° in amorphous ice deposited at low temperature, is the signature of such a distortion (compared with the angular distribution of HGW and cubic ice). Above 100 K, when amorphous ice progressively transforms into a phase similar to HGW, the distortion becomes barely visible. In summary, the deposition at very low temperature promotes a distortion of the hydrogen bond network without enhancement of the intrinsic density of the material (as indicated in Fig. 3, the average density is essentially constant, ~ 1.0 g/cm^3, whatever the temperature of deposition). By contrast, in HDA ice the distortion is generated by the amorphization

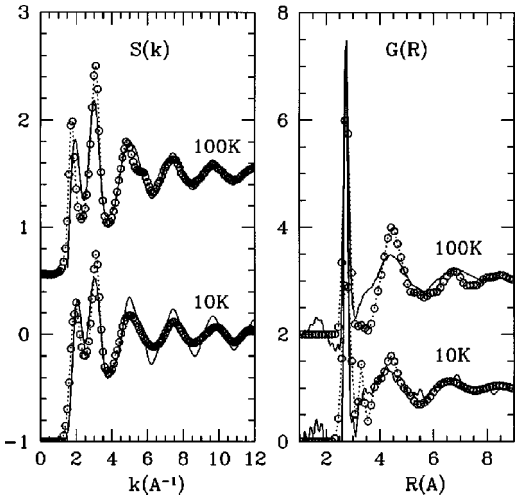

FIG. 11. X-ray structure factor and pair correlation function for ASW deposited on glassy water. The full curves are the simulation results at 10 and 100 K, respectively, and the circles are the data of Narten *et al.* (Ref. 42) for ASW deposited at 10 and 77 K, respectively. The dotted curves are just guidelines for the experimental data.

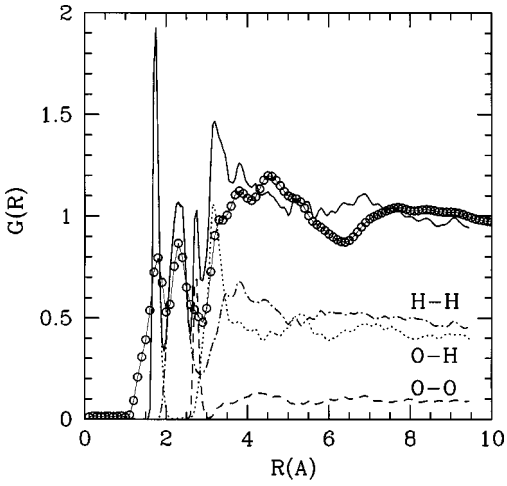

FIG. 12. The intermolecular pair correlation function for neutrons associated with ASW deposited on glassy water at 10 K. The decomposition of the total function (bold curve) into partial pair correlation functions (OO, OH, and HH) is also shown. The neutron data of Chowdhury *et al.* (Ref. 70) are represented by the circles and the thin curve.

of the crystal under pressure, a process that induces an increase in density ($0.94 \rightarrow 1.16$ g/cm^3).

In the case of our porous amorphous ice prepared by aggregation at 30 K, the evolution of the pdf and angular distribution function with the temperature is similar but not identical to that observed with vapor-deposited ice (see Figs. 9 and 10). Some differences are expected since, in the present case, the presence of voids and cages within the sample lowers the density, especially in the range 30–100 K (see Fig. 5). Although the pdf probes essentially the local environment (about three shells or 7–8 A) that is sensitive mainly to the intrinsic density of the material and less to its microporosity, the presence of a significant population of dangling OH bonds at the interfaces is visible on the pdf. Thus, at 30 K, one notices [Fig. 9(b)] a weakening of the hydrogen bond between a central molecule and its fourth neighbor with respect to what happens in dense ASW. In the same way the fifth molecule and the other ones are situated at a higher distance, meaning that the local structure in porous ASW loosens somewhat. However, the similarity of the local structure between nonporous and porous amorphous ice supports the idea that the intrinsic density of ASW is nearly constant ($\sim$1.0 g/cm^3) whatever the method of preparation (a related assertion has been reported in Ref. 67) and barely depends on the temperature of deposition or formation of the sample. This could explain some contradictory results in the literature when comparing data coming from different experimental techniques. For instance, optical techniques[34] and adsorption isotherm volumetry[68] are sensible to the ice porosity, infrared spectroscopy reveals the dangling OH bonds present at the free interfaces of the sample,[69] whereas x-ray and neutron scattering experiments give information essentially on the compact material.

To be complete it is worthwhile to compare our results with existing structural data for ASW made by deposition. The x-ray data of Narten *et al.*[42] are shown in Fig. 11, both in the reciprocal space and in the real space, and are compared with our simulation results. The experimental diffraction pattern and its evolution with temperature is qualitatively described by the simulation in spite of some deviation in the magnitude and width of the diffraction peaks. These deviations can be assigned partly to cut off effects in the simulation results due to the limited size of our samples. In the real space, the Fourier transform of the structure factor is given essentially by the oxygen–oxygen pdf and a very small contribution of the O–H pdf [for a discussion about the relationship between $S(k)$ and the pdfs see Ref. 58]. One notices in Fig. 11 that the interstitial peak is sharp and well resolved in the experimental function at 10 K when it appears as a shoulder in the calculation. In considering more recent diffraction data [see Fig. 2 in Ref. 44(b)], we believe that the sharp peak in the Narten data is an artifact and must be understood as an indication of a broad shoulder on the low-R flank of the second peak of the pdf. Besides, the sharp peak has disappeared from the experimental data when the ASW sample is heated from 10 to 77 K. Considering these uncertainties, the agreement between simulation and experiment can be considered as satisfying even if new x-ray data on vapor-deposited amorphous ice are certainly necessary.

Complementary information is given by neutron diffraction data that are more sensitive to hydrogen–hydrogen and oxygen–hydrogen correlations than to those for oxygen–oxygen. In Fig. 12 is presented the intermolecular pair correlation function for neutrons as obtained by Chowdhury *et al.*[70] for vapor-deposited ice at 10 K, and its comparison with our simulation data at the same temperature. As the total pair correlation function is a weighted sum of the atom–atom pdfs $[G(R) = 0.09 g_{\mathrm{OO}}(R) + 0.49 g_{\mathrm{OH}}(R) + 0.42 g_{\mathrm{HH}}(R)$, see the decomposition in the figure], a cancellation effect between the three contributions may enhance small differences in the total function. For this reason a good reproduction of the neutron structure data is a stringent test for the simulation. Thus the position of the numerous peaks is rather well reproduced by the simulation, but the magnitude of these

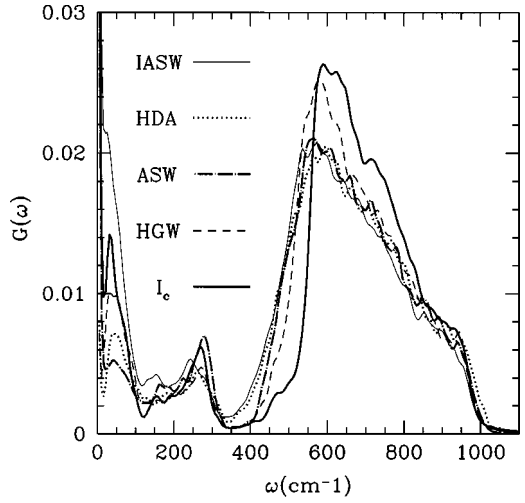

FIG. 13. Fourier transform of the vibrational density of states for hydrogen atoms in various amorphous ices and in cubic ice (see the text).

peaks are overestimated. Part of this discrepancy can be assigned to quantum effects that are not taken into account in the simulation and that tend to smooth the structure in real water,[71] especially at low temperature.[72]

Useful information on the hydrogen bond network in amorphous ices can be obtained from infrared absorption,[29,73–75] Raman scattering[76–78] and incoherent inelastic neutron scattering.[31,32,47,79] The latter technique gives a direct access to the vibrational density of states (VDOS) that sums up all kinds of intermolecular and intramolecular motions taking place in the solid. A majority of neutron scattering studies are focused on the intermolecular bands that cover the energy transfer range from a few meV (1 meV=8 cm^{-1}) to about 120 meV (or ~960 cm^{-1}) because these bands are intense and probe the rototranslational motions of the water molecules within the amorphous ice. A number of studies[31,32,47] have shown that the libration band (40–120 meV, or 320–960 cm^{-1}) is characteristic of the amorphous ice under consideration. Thus, the libration band associated with ASW is found to be in between that of HDA ice, located at a lower frequency, and that assigned to HGW, located at a higher frequency, all these libration bands being shifted toward lower frequencies with respect to the band associated with cubic ice. For this reason it is concluded[47] that the strength of the hydrogen bonds in the corresponding network follows the hierarchy Ic>HGW>ASW>HDA. To check whether the simulation is able to reproduce the above spectral feature, we have evaluated the power spectrum of the VDOS by taking the Fourier transform of the velocity time correlation function associated with hydrogen atoms (only these atoms are seen in an incoherent inelastic neutron scattering spectrum of water[31]), this result being multiplied by a prefactor accounting for a detailed balance. The results are presented in Fig. 13 for our vapor-deposited amorphous ice at 10 K and are compared with the spectrum for HDA ice at 50 K (previously evaluated in Ref. 46), HGW at 78 K, and cubic ice at 78 K, respectively. In the 400–600 cm^{-1} frequency range, the following order is observed in going from low to high frequency, HDA<ASW<HGW<Ic, an order consistent with experimental data (compare Fig. 13 with Fig. 2 in Ref. 47, with Fig. 4 in Ref. 31, and with Fig. 3 in Ref. 32). The fact that the libration band associated with ASW is found to be intermediate to HDA ice and HGW is expected after our previous discussion about the structure in amorphous ice. In our opinion, the low-frequency shift with respect to HGW is induced by the distortion of the hydrogen bond network taking place during the formation of the amorphous ice. To be complete notice also that our vapor-deposited amorphous ice at 10 K generates a power spectrum that is almost indistinguishable from the one produced by our amorphous cluster (not shown). Moreover, at higher temperature and especially above 100 K, the power spectrum of ASW shifts gradually toward that of HGW and becomes identical after annealing at Tg (not shown).

III. IRRADIATED ICE

A. Preamble

As discussed briefly in the Introduction, in the interstellar medium the cosmic ices are subjected to a variety of radiation depending on their environment. For example, comets stored in the Kuiper belt or in the Oort cloud are exposed to the galactic cosmic-ray environment (mostly isotropic). The latter one is estimated[80] to be composed of 87% protons, 12% helium nuclei, and 1% heavier nuclei, electrons being in much less proportion. Hence, radiation processing of ices exposed to cosmic rays is dominated by protons in the MeV range. Whatever the nature of the incident particles, an important quantity when dealing with radiation effects is the energy dose (eV per molecule or eV per m^2) deposited in the material. Thus, the external layers (0.1–0.5 m) of a comet stored in the Oort cloud for about 4.6×10^9 yr, is subjected to a cumulated irradiation dose[81] of ~600 eV/mol, a value that decreases to a few eV/mol in the deeper crust (~10 m). Dust particles coated with icy mantles are subjected to UV irradiation in addition to cosmic rays when they are within molecular clouds. Depending on the density of the cloud (the denser the cloud, the higher the UV attenuation), the energy dose due to UV photons can vary over a large range ($1-10^6$ eV/mol; see Ref. 80). Due to the small size of these icy grain mantles (~200 nm thick) the entire mantle is processed by irradiation. For many years a great number of studies were dedicated to reproducing in the laboratory the cosmic ices and the space environment involving UV or ion processing. A majority of these studies were concerned with the formation of complex organic molecules induced by irradiation and very few of them were dedicated to the structural modifications experienced by the ice itself under ion bombardment or UV photolysis. A notable exception is the observation of a transition from crystalline to amorphous ice induced by UV photons,[51] proton irradiation,[52] and ion bombardment.[53] However, to our knowledge, the structure of the resulting amorphous ice has not yet been described by diffraction experiments. On the other hand, it was discovered by cryoelectron microscopy[43,82] that an energetic electron beam causes the amorphization of cubic (or hexagonal) ice below 70 K, and that the electron dose required for this transition decreases drastically when the temperature decreases.

The analysis of the electron diffraction pattern also suggests that the recovered amorphous phase (called $I_a h$) could be of a higher density than the original ASW (called $I_a l$) when the latter one is deposited at a liquid nitrogen temperature. In the same way, at temperatures below 70 K, electron irradiation transforms $I_a l$ into $I_a h$. Notice that above ~90 K, cubic ice becomes resilient with respect to irradiation, while amorphous ice can be devitrified if a very high electron dose is used.[82] So in this context, it is worthwhile to investigate by MD simulation the behavior of an icy sample under irradiation and what kind of microscopic transformation occurs.

B. Method of computation

When irradiating a material, the choice of the radiation is not immaterial on the transformation undergone by the sample. UV photons on ice tend to break bonds, to ionize species, and to induce chemical reactions but the photon penetration is limited by optical attenuation. On the other hand, the effects generated by ion bombardment depend on the energy of the particles and of the stopping power of the ice. When a fast ion penetrates a solid, it loses its energy by two mechanisms:[83] by nuclear-elastic (knock-on) collisions and by electronic excitations and ionizations of the atoms. The stopping power (S) of a material, which is the energy loss per unit pathlength of the ion in the solid, can be approximated by the sum of a nuclear contribution plus an electronic contribution; $S = Sn + Se$.

The maximum of the nuclear stopping power for protons in ice is in the keV range while it is in the MeV range for the electronic contribution.[84] In the latter case, electronic excitations are responsible for a new phenomenon, the sputtering of ice,[85] for which molecules and ions can be ejected from the surface. Although this mechanism has important astrophysical implications,[86] it is outside the scope of the present study. For heavy ions (He^+,Ne^+,O^+,…), the electronic stopping power in the keV range and below, becomes negligible with respect to the nuclear one,[87] and only desexcitation by collisional cascade has to be taken into account. Since we are primarily interested in the transformation of ice structure under irradiation and not by the production and identification of new species, we restrict our model calculation to the bombardment by ions of relatively weak energy (less than 1 kev). In practice, we have submitted a lamella of glassy water and one of cubic ice, previously used for the deposition of water vapor, to the ion bombardment. However, if the energy of the incident ion is too large, its penetration depth may exceed the thickness of the lamella in leading to an unwanted sputtering of the target. So we have chosen a range of incident energy (10–100 eV) such that the penetration depth is smaller than the thickness of the lamella and, hence, all ions are stopped in the target. But in that case, called implantation-type experiment, the energy dose required to transform the ice is sufficiently high to consider the incident particles implanted in the target as a contaminating species that can blur the results (the bombarded target being at the end of the irradiation period a mixture of water and ions). To circumvent this problem we have bombarded the ice lamella with water molecules instead of ions. Notice that with our potential model for water, the molecules are rigid and nondissociable, so the incident molecules striking the target at very high velocity lose their energy only by elastic collisions with the water molecules of the target.

From a practical point of view, the MD simulations were performed with a lamella of glassy water (512 molecules) or cubic ice ($N = 432$) located at the middle of a parallelepipedic simulation cell. As before, periodic boundary conditions are used, and the equations of motion are solved within the microcanonical ensemble. The simulation starts by inserting a water molecule at a random location in each free volume situated on both sides of the target lamella. A high kinetic energy is assigned to each inserted molecules, the initial velocity being directed perpendicularly to the free surface of the lamella. By varying the energy of the incident molecules between 10 and 100 eV, it occurs that an energy of 35 eV (or 4.06×10^5 K in the temperature scale) was a good compromise between penetration length (~15 A) and thickness of the target (~40 A). An important parameter in an irradiation experiment is the energy dose deposited in the material (as long as the electronic contribution to the stopping power can be neglected). For a fixed energy of the incident particles (here 35 eV) the energy dose deposited is simply proportional to the number of effective events for which the energy of the incident particle is yielded to the material. In the simulation, as for a real irradiation experiment, as soon as the energetic particle strikes the lamella, a cascade of collisions is initiated, where recoiling atoms absorb part of the incident energy. This leads to a transient increase of the temperature along the track core, a heating that is finally dissipated by thermal diffusion through the material. However, for a system of limited size such as the simulated one, it is crucial to restrict the thermal excess to the track core and avoiding that it propagates to the entire icy sample. A simple way to proceed is to rescale the velocities of all the molecules of the target (except the one of the incident particle) at each MD step to keep constant the temperature of the lamella. Other procedures are possible, as, for example, to make the lamella in contact with a thermal bath through an adjustable coupling constant to mimic heat conduction (e.g., in Ref. 88), but we believe that our simple method is sufficient for a first attempt. In proceeding that way the temperature associated with the molecules surrounding the track core is transiently very high while that corresponding to remote molecules is very low in order to keep constant the average temperature of the lamella. For illustration is presented in Fig. 14 the time evolution of the kinetic energy distribution function of the molecules of a glassy lamella maintained at 50 K during a collision event. One sees that the maximum of the distribution shifts toward lower energy (cooling) between time zero and $t = 100\Delta t$ (where $\Delta t = 0.5$ fs) and then shifts in the opposite direction (toward higher energies) between $100\Delta t$ and $4000\Delta t$ [see the sequence (a), (b), (c), and (d) in the figure]. Correspondingly, the energy range between 2.10^2 and 10^4 K becomes densely populated in the distribution function at short time [see curve (c) in the figure] due to the excitations of the molecules along the track core, and diminishes gradually at longer times. However, several picoseconds are necessary for the system to recover thermal equilibrium.

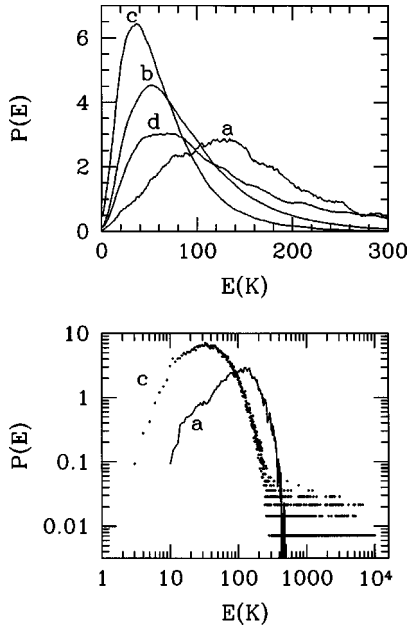

FIG. 14. Evolution with time of the kinetic energy distribution function for a glassy lamella maintained at 50 K and bombarded with a 35 eV water molecule. Curve (a) is 10 MD steps after the event, curve (b) is 30 MD steps after the event, curve (c) is 100 MD steps after the event, and (d) is 4000 MD steps after the event. The results are shown in a linear plot in the upper panel and in a log–log plot in the lower panel. In the latter case only curves (a) (see bold line) and (c) (see dots), are shown for convenience. In curve (c), notice the important population in the tail of the distribution at high energy due to the thermal excitation of the molecules along the track core.

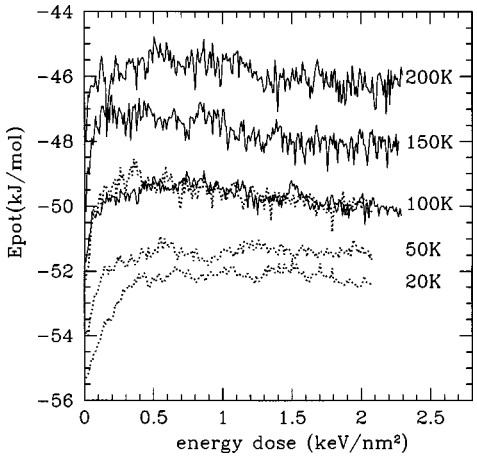

FIG. 15. Evolution of the potential energy of a glassy lamella (full curves) and of a crystalline lamella (dotted curves) with the energy dose received during the bombardment by 35 eV water molecules. The evolution is shown for different temperatures.

From a more general point of view, it is noteworthy that the kind of MD simulations presented here to model ion bombardment is not completely new. In the last decade an abundant literature was devoted to the study by computer simulation of radiation damage in metals and ceramics.[88–95] Thus, when a knock-on atom strikes a metal, it induces by displacement cascades point defects and local disordering that affect the properties of the material. In some cases the radiation damages are so important that the metal or the ceramic under irradiation is amorphized, a case currently investigated by MD simulations[96–98] and that shares several common features with the present study (see also the footnote[99]).

C. Results

To study irradiation effects on amorphous and cubic ice we have bombarded our target lamella with 35 eV water molecules at a rate of 1 strike per 10^3 MD steps on each Z side of the icy sample. Very scarcely an incident molecule rebounds on the surface of the target or causes a significant sputtering in penetrating the target, but these events have no important consequences on the results. The irradiation of cubic ice has been performed at 20, 50, and 100 K, and that of amorphous ice at 20, 50, 100, 150, and 200 K, respectively. The evolution of the potential energy of the lamella with the energy dose (expressed in keV/nm^2) deposited in the material is shown in Fig. 15. One sees that after a rapid increase, the potential energy becomes invariant with the energy dose and so, whatever the temperature and the initial morphology of the lamella. When the bombardment sequence is interrupted, the irradiated samples present a short period of energy relaxation (of the order of 100 ps), the final values being significantly higher than those associated with the nonirradiated sample except at 200 K, where no significant change is observed (not shown). In fact, the potential energy of the irradiated sample is generally higher (not shown) than that associated with vapor-deposited amorphous ice presented in Fig. 8. These findings suggest that below the glass transition temperature, the structure of the ice is deeply modified by the bombardment. Actually, and this is an important result of the present study, the amorphous ice densifies upon irradiation while cubic ice amorphizes into a phase denser than the original crystal (see Fig. 16 for a snapshot of the crystal after irradiation). This is illustrated in Fig. 17, where the average density of the irradiated samples is presented as function of temperature. Notice that the central part of the lamella ($\sim$10 A thick; see Fig. 16) is beyond the penetration length of the incident particles, and consequently this part was not taken into account for the density evaluation. The density is found significantly enhanced by irradiation whatever the temperature, but the higher the temperature the lower the density. Moreover, the value of the density after irradiation is independent of the original phase of the ice (amorphous or crystalline). Above the glass transition temperature there is virtually no densification, as expected. As far as the amorphization of cubic ice is concerned, we have not pursued our investigation above 100 K, but we believe that the amorphization process might be effective at a higher temperature. This seems to contradict the experimental data,[43,51,52,82] which indicate that the amorphization of crystalline ice is not observed above 90 K whatever the kind of radiation used. As a matter of fact, a commonly accepted explanation is that irradiation tends to create defects in the lattice at any temperature, but at high enough temperature a restoration mechanism (activated process) takes place and renders the crystal insensitive to irradiation effects (for a discussion see Ref. 97). In the present case, we believe that the quenching mechanism applied during the simulation to keep constant the temperature is so drastic that the crystal

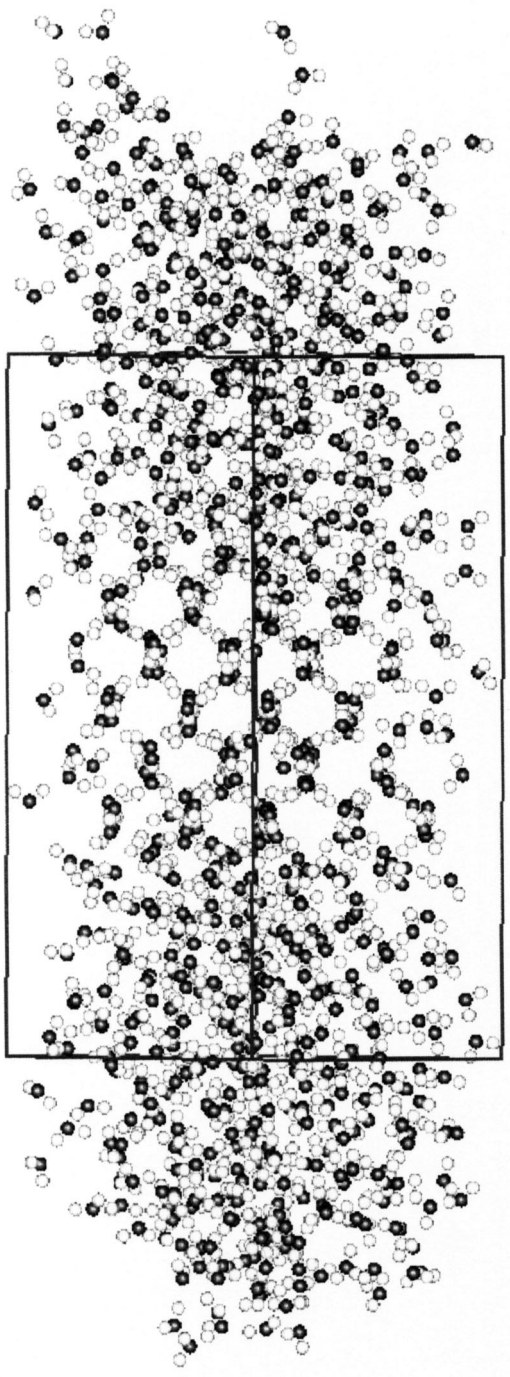

FIG. 16. Snapshot of a sample of cubic ice after the bombardment by 432 water molecules. The boundary of the sample of cubic ice before irradiation is indicated by the bold lines.

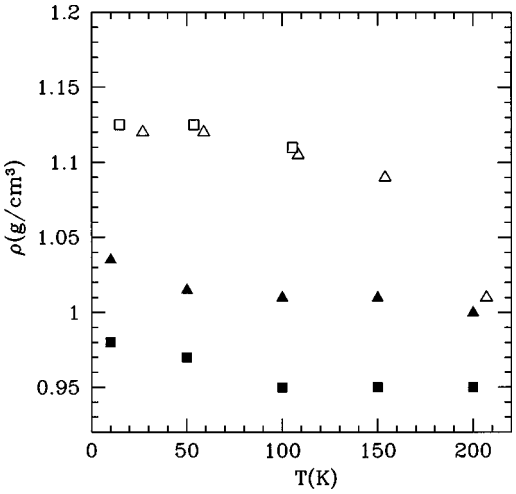

FIG. 17. Evolution of the density of irradiated ice with temperature. The empty triangles are for the irradiated sample of glassy water and the empty squares are for the irradiated sample of cubic ice, respectively, while the full triangles and full squares correspond to the density of the glassy and crystalline sample before irradiation.

does not have enough time to repair itself between two successive events. In the same way the number of implanted molecules becomes very significant when the irradiation persists, a feature that certainly prevents the restoration mechanism to be very effective. Clearly, other simulation techniques have to be considered in that case.

However that may be, the important thing is that the simulation reproduces the irradiation-induced amorphization of cubic ice at low temperature and predicts, in addition, that the recovered amorphous sample is as dense as HDA ice made by pressurizing crystalline ice at liquid nitrogen temperature. A scenario for such an amorphization-densification process is the following. Along the trajectory of the impinging molecule the surrounding molecules are heated well above the melting temperature (and above the critical temperature as well). The corresponding hydrogen bonds are transiently broken as occurs in dense supercritical water when the temperature is higher than 1000 K (for a detailed discussion see Ref. 58), although the molecules remain confined by the packing of the ice all around them. The thermal spike vanishes in a few picoseconds by collision cascades with the other molecules of the sample, the net result being a quenching rate of the molecules of the track core as large as 10^{15} K/s. These molecules are then trapped in a configuration of high energy corresponding to a distorted hydrogen bond network denser than the original one. To quantify this picture we have evaluated the oxygen–oxygen pair distribution function associated with our irradiated samples, by excluding from the counting the molecules located on the free interfaces and those situated within the central layers of the lamella that were not affected by the bombardment. The results for the irradiated glassy sample are presented in Fig. 18 at different temperatures, while those for the irradiated cubic ice are not shown because they are essentially indistinguishable from the former ones. It is clear that the lower the temperature, the more prominent is the interstitial peak around 3.4 A. The close resemblance of this feature with the one exhibited by HDA ice, also shown in the figure, is striking (see also Fig. 13 in Ref. 46 and compare). In the same way, the signature of the distortion of the hydrogen bond network is clearly apparent in the O–O–O angular distribution between a central molecule and its four nearest neighbors (see Fig. 19). Like with HDA ice, the angular distribution of irradiated ice exhibits a pronounced shoulder around 80°. In summary, a high-density amorphous ice very similar structurally to HDA ice can be formed at low pressure by molecular bombardment.

Additional information is provided by the vibrational

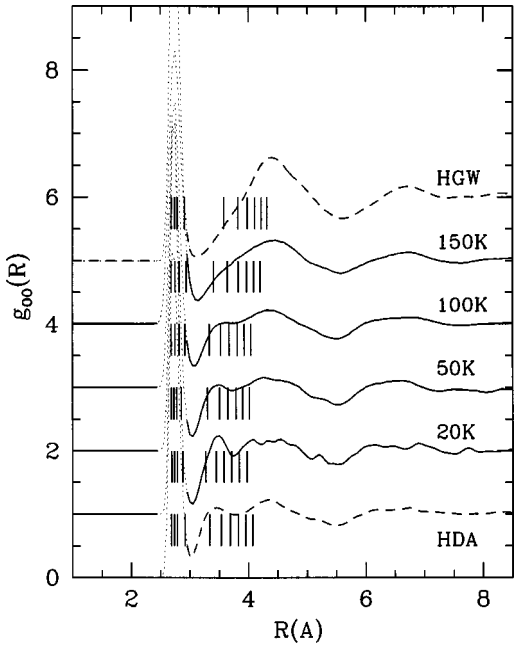

FIG. 18. The same as in Fig. 9, but for the irradiated sample of glassy water at different temperatures.

density of state associated with the hydrogen atoms. In Fig. 13 the power spectrum of the VDOS for irradiated amorphous ice (IASW) at 100 K is compared with that of HDA ice, glassy water, and cubic ice, respectively. The simulation predicts that an inelastic neutron scattering spectrum of ion-irradiated ice should be virtually identical to that of HDA ice.

As evoked earlier, there are very few experimental studies devoted to the investigation of the ice transformation under irradiation.[43,51–53,82] Among these, one work is particularly relevant for our purpose,[53] where the ice is irradiated with He^+ ions in the keV range for which electronic excitations are negligible, a situation close to the simulation conditions. In this work, the structure of the irradiated ice is probed by infrared spectroscopy in the frequency region corresponding to the OH band. The amorphous ice recovered after irradiation of cubic ice at 10 K presents a band shape very similar to that exhibited by vapor-deposited amorphous ice (ASW) at about the same temperature. Unfortunately, the data are not accurate enough to give more detailed information on the structure of this ice. We hope that the present simulation study will promote new experimental work in the near future.

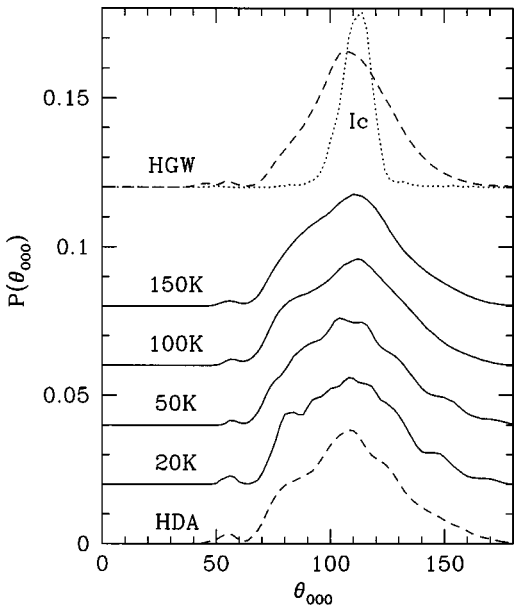

FIG. 19. The same as in Fig. 10, but for the irradiated sample of glassy water at different temperatures.

IV. CONCLUSION

With the purpose of clarifying a number of points raised in the experimental literature, we have investigated by molecular dynamics simulation the thermodynamics, the structure, and the vibrational properties of vapor-deposited amorphous ice (ASW) as well as the phase transformations experienced by crystalline and amorphous ice under ion bombardment. Concerning ASW, we have shown that by changing the conditions of the deposition process, it is possible to form either a nonporous amorphous deposit whose density ($\sim$1.0 g/cm^3) is essentially invariant with the temperature of deposition, or a microporous sample whose density varies drastically upon temperature annealing (the higher the temperature, the larger the density). It is also found that ASW is energetically different from glassy water, except at the glass transition temperature and above. However, the analysis of the microscopic structure of the simulated samples suggests that the hydrogen bond network in the compact material is mostly independent of the microporosity of the amorph at a given temperature, even if the average density can be very different. On the other hand, the temperature of formation is found to be a key parameter for the properties of amorphous ice. Thus, at very low temperatures ($T \leqslant 50$ K), the oxygen–oxygen pair distribution function exhibits a shoulder at about 3.4 A, a feature highly reminiscent of the interstitial peak characterizing HDA ice and investigated previously.[46] In the same way the vibrational properties of ASW are found to be closer to that exhibited by HDA ice than to those associated with HGW. A low temperature of deposition favors the building of a distorted hydrogen bond network characterized by a significant deviation from the tetrahedral configuration, whereas on average each water molecule is hydrogen bonded to its four nearest neighbors. The fact that ASW, deposited at very low temperature, and HDA ice share some common structural features in spite of a completely different process of formation, sheds light on the controversy about the existence of a high-density phase made by vapor deposition. One is tempted to say that the simulation results presented here close the discussion in demonstrating that vapor-deposited amorphous ice at very low temperature is not as high a density phase as HDA ice (its density is $\sim$1.0 g/cm^3 instead of $\sim$1.16 g/cm^3), although its hydrogen bond network shows the same kind of angular distortion. On one hand the distortion is generated by the low temperature of deposition while, on the other hand, the distortion results from the pressure-induced amorphization of the crystal. Moreover, it is found that the excess enthalpy (and entropy) of ASW with respect to cubic ice increases

drastically when the temperature of deposition is decreasing. The astrophysical implication of this finding is that the evaporation rate of interstellar amorphous ices are likely many orders of magnitude greater than that of their corresponding crystalline analogs, which may reduce their lifetime significantly.

In order to model the processing of interstellar ices by cosmic ray protons and heavy ions coming from the magnetospheric radiation environment around the giant planets, we have bombarded samples of amorphous ice and cubic ice with 35 eV water molecules. In this energy range the nuclear stopping power (collision cascades) dominates inelastic electronic absorption, which justifies the use of molecular dynamics calculations. An important simulation result is that after irradiation the recovered samples are found to be densified by the bombardment; the lower the temperature, the higher the density of the recovered sample. This densification is induced by the very fast quenching rate experienced by the molecules along the track core after the local temperature has been raised well above the critical temperature by collision cascade. It is noteworthy that vitreous silica is also known to densify under irradiation.[100,101] Here also the rapid cooling that follows irradiation is found to be responsible for the densification.[102] Furthermore, when the ice under irradiation is crystalline, the sample thickness corresponding to the penetration length becomes amorphous and shows a density very similar to the one obtained when irradiating a sample of amorphous ice. The analysis of the structure and vibrational properties of this new high-density phase of amorphous ice shows a close relationship with those of HDA ice. Thus, it appears that the irradiation of amorphous or crystalline ice at low temperature by heavy ions of low energy (in the keV range) is a third way to produce a high-density amorphous phase of ice, after the well-known pressure-induced amorphization of ice I and the hyperquenching of liquid water maintained under pressure (for a brief review see Sec. I in Ref. 46). So the observation of this phase in the laboratory could be important to improve our understanding of the phase diagram of low-temperature water and to better predict the evolution of cosmic ices in the interstellar medium.

[1] E. F. Burton and W. F. Oliver, Nature (London) **135**, 505 (1935).
[2] J. Klinger, J. Phys. Chem. **87**, 4209 (1983).
[3] A. Kouchi, T. Yamamoto, T. Kosaza, T. Kuroda, and J. M. Greenberg, Astron. Astrophys. **290**, 1009 (1994).
[4] S. A. Stern, in *Solar System Ices*, edited by B. Schmidtt *et al.* (Kluwer Academic, Dordrecht, 1998), p. 685.
[5] M. E. Bailey, Science **296**, 2151 (2002).
[6] C. Chyba and C. Sagan, Nature (London) **355**, 125 (1992).
[7] E. L. Gibb, D. C. B. Whittet, W. A. Schutte *et al.*, Astrophys. J. **536**, 347 (2000).
[8] A. G. G. M. Tielens, W. Hagen, and J. M. Greenberg, J. Phys. Chem. **87**, 4220 (1983).
[9] J. P. Bradley, Science **265**, 925 (1994).
[10] J. Crovisier, K. Leech, D. Bockelée-Morvan, T. Y. Brooke, M. S. Hanner, B. Altieri, H. U. Keller, and E. Lellouch, Science **275**, 1904 (1997).
[11] R. L. Hudson and M. H. Moore, J. Geophys. Res. **106**, 33275 (2001).
[12] P. Ehrenfreund, L. d'Hendecourt, S. Charnley, and R. Ruiterkamp, J. Geophys. Res. **106**, 33291 (2001).
[13] P. Ehrenfreund, Science **283**, 1123 (1999).
[14] M. P. Bernstein, S. A. Sandford, L. J. Allamandola, J. S. Gillette, S. J. Clemett, and R. N. Zare, Science **283**, 1135 (1999).
[15] W. L. Brown, L. J. Lanzerotti, and R. E. Johnson, Science **218**, 525 (1982).
[16] P. A. Gerakines, W. A. Schutte, J. M. Greenberg, and E. F. van Dishoeck, Astron. Astrophys. **296**, 810 (1995).
[17] P. A. Gerakines, W. A. Schutte, and P. Ehrenfreund, Astron. Astrophys. **312**, 289 (1996).
[18] G. Strazzulla, in Ref. 4, p. 281.
[19] F. Salama, in Ref. 4, p. 259.
[20] D. A. Bahr, M. Fama, R. A. Vidal, and R. A. Baragiola, J. Geophys. Res. **106**, 33285 (2001).
[21] P. A. Gerakines, M. H. Moore, and R. L. Hudson, J. Geophys. Res. **106**, 33381 (2001).
[22] M. P. Bernstein, J. P. Dworkin, S. A. Sandford, G. W. Cooper, and L. J. Allamandola, Nature (London) **416**, 401 (2002).
[23] G. M. Munoz Caro, U. J. Meierhenrich, W. A. Schutte, B. Barbier, A. A. Segovia, H. Rosenbauer, W. H.-P. Thiemann, A. Brack, and J. M. Greenberg, Nature (London) **416**, 403 (2002).
[24] J. A. McMillan and S. C. Los, Nature (London) **206**, 806 (1965).
[25] M. Sugisaki, H. Suga, and S. Seki, Bull. Chem. Soc. Jpn. **41**, 2591 (1968).
[26] P. Brügeller and E. Mayer, Nature (London) **288**, 569 (1980).
[27] A. Hallbrucker, E. Mayer, and G. P. Johari, J. Phys. Chem. **93**, 4986 (1989).
[28] E. Mayer and P. Brügeller, Nature (London) **298**, 715 (1982).
[29] E. Mayer, J. Phys. Chem. **89**, 3474 (1985).
[30] G. P. Johari, A. Hallbrucker, and E. Mayer, J. Chem. Phys. **95**, 2955 (1991).
[31] A. J. Kolesnikov, J. Li, S. F. Parker, R. S. Eccleston, and C. K. Loong, Phys. Rev. B **59**, 3569 (1999).
[32] O. Yamamuro, Y. Madokoro, H. Yamasaki, T. Matsuo, I. Tsukushi, and K. Takeda, J. Chem. Phys. **115**, 9808 (2001).
[33] E. Mayer and R. Pletzer, J. Chem. Phys. **80**, 2939 (1984).
[34] B. S. Berland, D. E. Brown, M. A. Tolbert, and S. M. George, Geophys. Res. Lett. **22**, 3493 (1995).
[35] D. E. Brown, S. M. George, C. Huang, E. K. L. Wong, K. Brider, R. S. Smith, and B. D. Kay, J. Phys. Chem. **100**, 4988 (1996).
[36] I. Engqvist, I. Lundström, B. Liedberg, A. N. Parikh, and D. L. Allara, J. Chem. Phys. **106**, 3038 (1997).
[37] S. Trakhtenberg, R. Naaman, S. R. Cohen, and I. Benjamin, J. Phys. Chem. B **101**, 5172 (1997).
[38] K. P. Stevenson, G. A. Kimmel, Z. Dohnàlek, R. S. Smith, and B. D. Kay, Science **283**, 1505 (1999).
[39] G. A. Kimmel, K. P. Stevenson, Z. Dohnàlek, R. S. Smith, and B. D. Kay, J. Chem. Phys. **114**, 5284 (2001).
[40] Z. Dohnàlek, G. A. Kimmel, P. Ayotte, R. S. Smith, and B. D. Kay, J. Chem. Phys. **118**, 364 (2003).
[41] M. S. Westley, G. A. Baratta, and R. A. Baragiola, J. Chem. Phys. **108**, 3321 (1998).
[42] A. H. Narten, C. G. Vankatesh, and S. A. Rice, J. Chem. Phys. **64**, 1106 (1976).
[43] H.-G. Heide, Ultramicroscopy **14**, 271 (1984); H.-G. Heide and E. Zeitler, *ibid.* **16**, 151 (1985).
[44] P. Jenniskens and D. F. Blake, Science **265**, 753 (1994); P. Jenniskens, D. F. Blake, M. A. Wilson, and A. Pohorille, Astrophys. J. **455**, 389 (1995).
[45] O. Mishima, L. D. Calvert, and E. Whalley, Nature (London) **310**, 393 (1984); **314**, 76 (1985).
[46] B. Guillot and Y. Guissani, J. Chem. Phys. **119**, 11740 (2003).
[47] A. I. Kolesnikov, J.-C. Li, S. Dong, I. F. Bailey, R. S. Eccleston, W. Hahn, and S. F. Parker, Phys. Rev. Lett. **79**, 1869 (1997).
[48] A. Givan, A. Loewenschuss, and C. J. Nielsen, J. Phys. Chem. B **101**, 8696 (1997).
[49] N. Horimoto, H. S. Kato, and M. Kawai, J. Chem. Phys. **116**, 4375 (2002).
[50] J. Dubochet and J. Lepault, J. Phys. C **45**, 85 (1984).
[51] A. Kouchi and T. Kuroda, Nature (London) **344**, 134 (1990).
[52] M. H. Moore and R. L. Hudson, Astrophys. J. **401**, 353 (1992).
[53] G. A. Baratta, G. Leto, F. Spinella, G. Strazzulla, and G. Foti, Astron. Astrophys. **252**, 421 (1991); G. Strazzulla, G. A. Baratta, G. Leto, and G. Foti, Europhys. Lett. **18**, 517 (1992).
[54] Q. Zhang and V. Buch, J. Chem. Phys. **92**, 1512 (1990); **92**, 5004 (1990); V. Buch, *ibid.* **93**, 2631 (1990); V. Buch and J. P. Devlin, *ibid.* **94**, 4091 (1991); V. Buch, *ibid.* **96**, 3814 (1992).
[55] U. Essmann and A. Geiger, J. Chem. Phys. **103**, 4678 (1995).
[56] M. A. Wilson, A. Pohorille, P. Jenniskens, and D. F. Blake, Origins Life Evol. Biosphere **25**, 3 (1995).
[57] B. Guillot, J. Mol. Liq. **101/1–3**, 219 (2002).

[58] B. Guillot and Y. Guissani, J. Chem. Phys. **114**, 6720 (2001).
[59] J. Alejandre, D. J. Tildesley, and G. A. Chapela, J. Chem. Phys. **102**, 4574 (1995).
[60] S. W. Levine, J. R. Engstrom, and P. Clancy, Surf. Sci. **401**, 112 (1998); G. A. Kimmel, Z. Dohnàlek, K. P. Stevenson, R. S. Smith, and B. D. Kay, J. Chem. Phys. **114**, 5295 (2001).
[61] G. P. Johari, J. Chem. Phys. **102**, 6224 (1995).
[62] K. Takeda, O. Yamamuro, and H. Suga, J. Phys. Chem. **99**, 1602 (1995).
[63] R. J. Speedy, P. G. Debenedetti, R. S. Smith, C. Huang, and B. D. Kay, J. Chem. Phys. **105**, 240 (1996).
[64] A. Kouchi, Nature (London) **330**, 550 (1987).
[65] A. Kouchi, J. Cryst. Growth **99**, 1220 (1990).
[66] N. J. Sack and R. A. Baragiola, Phys. Rev. B **48**, 9973 (1993).
[67] P. Jenniskens, D. F. Blake, and A. Kouchi, in Ref. 4, p. 139.
[68] C. Manca, C. Martin, and P. Roubin, Chem. Phys. Lett. **364**, 220 (2002).
[69] J. P. Devlin, J. Sadlej, and V. Buch, J. Phys. Chem. A **105**, 974 (2001).
[70] M. R. Chowdury, J. C. Dore, and J. T. Wenzel, J. Non-Cryst. Solids **53**, 247 (1982).
[71] B. Guillot and Y. Guissani, J. Chem. Phys. **108**, 10162 (1998).
[72] H. Gai, G. K. Schenter, and B. C. Garett, Phys. Rev. B **54**, 14873 (1996).
[73] A. H. Hardin and K. B. Harvey, Spectrochim. Acta, Part A **29**, 1139 (1973).
[74] M. S. Bergren, D. Schuh, M. G. Sceats, and S. A. Rice, J. Chem. Phys. **69**, 3477 (1978).
[75] W. Hagen, A. G. G. M. Tielens, and J. M. Greenberg, Chem. Phys. **56**, 367 (1981); W. Hagen and A. G. G. M. Tielens, Spectrochim. Acta, Part A **38**, 1089 (1982).
[76] T. C. Sivakumar, S. A. Rice, and M. G. Sceats, J. Chem. Phys. **69**, 3468 (1978).
[77] H. Kanno, K. Tomikawa, and O. Mishima, Chem. Phys. Lett. **293**, 412 (1998).
[78] C. A. Tulk, D. D. Klug, R. Branderhorst, P. Sharpe, and J. A. Ripmeester, J. Chem. Phys. **109**, 8478 (1998).
[79] D. D. Klug, E. Whalley, E. C. Svensson, J. H. Root, and V. F. Sears, Phys. Rev. B **44**, 841 (1991).
[80] M. H. Moore, R. L. Hudson, and P. A. Gerakines, Spectrochim. Acta, Part A **57**, 843 (2001).
[81] G. Strazulla and R. E. Johnson, in *Comets in the Post-Halley Era*, edited by R. Newburn, Jr., M. Neugebauer, and J. Rahe (Kluwer, Dordrecht, 1991), p. 243.
[82] J. Lepault, R. Freeman, and J. Dubochet, J. Microsc. **132**, RP3 (1983).
[83] I. G. Kaplan and A. M. Miterev, Adv. Chem. Phys. **68**, 255 (1987).
[84] J. F. Ziegler, J. P. Biersack, and U. Littmark, *The Stopping and Range of Ions in Solids* (Pergamon, New York, 1985).
[85] W. L. Brown, L. J. Lanzerotti, and R. E. Johnson, Science **218**, 525 (1982).
[86] R. E. Johnson, Rev. Mod. Phys. **68**, 305 (1996).
[87] A. Bar-Nun, G. Herman, M. L. Rappaport, and Y. Mekler, Surf. Sci. **150**, 143 (1985).
[88] F. Gao, D. J. Bacon, P. E. J. Flewitt, and T. A. Lewis, J. Nucl. Mater. **249**, 77 (1997).
[89] T. Diaz de la Rubia and G. H. Gilmer, Phys. Rev. Lett. **74**, 2507 (1995).
[90] J. M. Perlado, J. Nucl. Mater. **251**, 98 (1997).
[91] D. J. Bacon, F. Gao, and Y. N. Osetsky, Nucl. Instrum. Methods Phys. Res. B **153**, 87 (1999).
[92] D. J. Bacon, F. Gao, and Y. N. Osetsky, J. Nucl. Mater. **276**, 1 (2000).
[93] A. V. Barashev, D. J. Bacon, and S. I. Golubov, J. Nucl. Mater. **276**, 243 (2000).
[94] L. Malerba, J. M. Perlado, A. Sanchez-Rubio, I. Pastor, L. Colombo, and T. Diaz de la Rubia, J. Nucl. Mater. **283–287**, 794 (2000).
[95] T. Aoki, S. Chiba, J. Matsuo, I. Yamada, and J. P. Biersack, Nucl. Instrum. Methods Phys. Res. B **180**, 312 (2001).
[96] M. Spaczér, A. Caro, and M. Victoria, Phys. Rev. B **52**, 7171 (1995).
[97] L. Malerba and J. M. Perlado, J. Nucl. Mater. **289**, 57 (2001).
[98] X. Yuan, V. Pulim, and L. W. Hobbs, J. Nucl. Mater. **289**, 71 (2001).
[99] To check whether the use of water molecules as incident energetic particles could bias the results, we have modeled irradiation effects with another procedure related to that commonly used to simulate recoiling atoms in metal and ceramics. In this case, a water molecule of the glassy lamella is chosen at random to which is assigned a high velocity pointing toward the middle of the lamella and corresponding to a kinetic energy of 35 eV. To maintain a constant temperature of the system, the velocities of all the molecules (except that of the energetic particle) are rescaled at each of the MD steps until all the excess energy of the energetic particle is dissipated by collisions with the molecules of the lamella. The procedure of choosing a new molecule as energetic particle is repeated every 10^3 MD steps until each molecule of the lamella has been processed. The results of these calculations are essentially the same as those obtained with the implantation simulation in which the lamella is bombarded with 35 eV water molecules. In particular, the densification of amorphous ice is obtained and the recovered sample present the same structural properties as those described afterward in the text with the implantation technique.
[100] W. Primak, Phys. Rev. A **133**, 531 (1958); W. Primak and R. Kampwirth, J. Appl. Phys. **39**, 5651 (1968).
[101] C. Fiori and R. A. B. Devine, Phys. Rev. B **33**, 2972 (1986).
[102] A. Wooton, B. Thomas, and P. Harrowell, J. Chem. Phys. **115**, 3336 (2001).